

Article

Healable, Flexible Supercapacitors Based on Shape Memory Polymers

Huankai Zhou, Hongsheng Luo *, Xingdong Zhou, Huaquan Wang, Yangrong Yao, Wenjing Lin and Guobin Yi

Faculty of Chemical Engineering and Light Industry, Guangdong University of Technology, 510006 Guangzhou, China; zhouhk816@163.com (H.Z.); zxd52013149898@163.com (X.Z.); whq931@163.com (H.W.); 13425414239@163.com (Y.Y.); jingjingfable@126.com (W.L.); ygb702@163.com (G.Y.)

* Correspondence: hongshengluo@163.com

Received: 20 August 2018; Accepted: 18 September 2018; Published: 25 September 2018



Abstract: Supercapacitors as novel and efficient energy storage devices could provide a higher power density and energy density compared to other electronics and devices. However, traditional supercapacitors are readily damaged, which leads to degraded performance or even failure. To make them more durable and efficient, healable flexible shape memory-based supercapacitors were unprecedentedly explored by a transfer process, in which the conductive nano-carbon networks were decorated with pseudocapacitance materials, followed by embedding them into a shape memory polymer matrix containing healing reagents. The composite exhibited flexibility, supercapacitance and self-healing capability originating from the shape memory effect and healing reagent. The morphologies, thermal, mechanical and capacitive properties, and the self-healability of the composite were investigated. In particular, the influence of the compositions on the healing efficiency was considered. The optimized composite exhibited good capacitance (27.33 mF cm^{-1}), stability (only 4.08% capacitance loss after 1500 cycles) and healable property (up to 93% of the healing efficiency). The findings demonstrated how to endow the flexible polymeric electronics with healable bio-mimetic properties and may greatly benefit the application of intelligent polymers in the field of multi-functional electrical materials.

Keywords: healability; supercapacitors; shape memory; carbon nanotubes; flexibility

1. Introduction

Self-healable polymers, as one of the most important bio-mimetic materials, have been widely exploited for several decades. The shape memory-assisted self-healing (SMASH) approach proposed in 2009 enabled externally visible cracks to be healed, prolonging the life of polymeric materials [1]. For the traditional self-healing polymers, mechanisms include self-healing effects were achieved via different approaches such as micro-capsules and Diels-Alder reactions. Compared to the traditional self-healing polymers, the SMASH acts as a novel mechanism, including healing reagents and shape recovery to make the cracks interface close up and become more adhesive. Due to the excellent performance, SMASH has been widely reported [2–5].

With the development of wearable and portable electronics, flexibility has played an important role in energy storage devices [6–8]. Compared to batteries and conventional capacitors, supercapacitors (SCs) as novel and wearable storage devices can make up for the shortcomings of traditional devices and provide a higher power density than that of batteries and a higher energy density than that of conventional capacitors. Thus, flexible SCs have become important energy storage devices. Furthermore, with the demand for increasing storage, lots of different flexible SCs have been invented. However, most SCs are vulnerable to external physical damage and could not be repaired. Therefore,

the remarkable reliability of epidermal electronics and intelligent textiles is required in case of mechanical damage. Smart energy-storage devices such as self-healable supercapacitors [9–13], having excellent healable electrochemical performance, are believed to well meet the requirement. However, most of the self-healing was achieved by hydrogen bonding [9–11], magnetism [12], or coordination [13] and some of these are the reversible interaction processes.

In comparison, the shape memory-assisted self-healable polymers could restore larger cracks and physical damage. Furthermore, there is a simple method to fabricate a self-healable composite. Inspired by these facts, herein we fabricated a self-healable, flexible and conductive composite based on shape memory polymers. According to our previous reports on the nano carbon-containing shape memory polymer composite [14–16], the functional flexible electronics exhibiting electro-trigger shape memory behaviors and temperature/water stimuli sensing peculiarity were explored. The SMP is quite attractive as a mechanical support and current collector because of its superior properties such as softness and repeated deformations [1]. Additionally, carbon nanotubes with large specific surface area and special hollow structure are loaded with MnO₂, which acts as an excellent active material in supercapacitors [17–20]. The prepared MnO₂/CNT/PCL/SMPU composite is denoted as MCP_xS_y, where x and y are the mass percent of PCL and SMPU, respectively. In our work, we found that the MCP40S60 showed the best flexibility and good healing efficiency. Electrochemical measurements demonstrated that the MCP40S60 composite exhibited a good capacitance of 27.33 mF cm⁻¹ and good cycle performance (only 4.08% capacitance loss after 1500 cycles). Importantly, the MCP40S60 retained 93% capacitance after the composite was repaired. The composite not only had excellent capacitance but also was a flexible and healable smart material.

2. Materials and Methods

Potassium permanganate (KMnO₄, 99.5 wt %), sodium sulphate (Na₂SO₄, 99.5 wt %) and *n,n*-dimethylacetamide (DMAc, 99.8 wt %) were bought from Tianjin Damao Chemical Reagent Factory. Multi-walled carbon nanotube (CNT, 99.0 wt %) was bought from Nanjing Jicang Nano Technology Co. Ltd. (Nanjing, China) Polycaprolactone (PCL, Mn = 80,000 g mol⁻¹), sulfuric acid (H₂SO₄, 98.0 wt %), and nitric acid (HNO₃, 68.0 wt %) were purchased from Sigma (Shanghai, China). Polyvinyl alcohol (PVA, Mn = 75,000–80,000 g mol⁻¹) was bought from Sinopharm Chemical Reagent Co. Ltd. (Shanghai, China). The crystalline SMPU was synthesized with PCL/DMI and BDO [21].

The MnO₂/CNT film was synthesized with the multi-walled CNT and acidic KMnO₄ solution [19]. The reaction is as follows:



Firstly, CNTs were treated with a mixture of H₂SO₄ and HNO₃ (the volume ratio was 3:1) for 3.5 h and were filtered and washed by deionized water until they became neutral. The 80 mg as-prepared CNTs were dispersed in 100 mL 0.1 M H₂SO₄ solution with ultrasound for 0.5 h. Then, 60 mg KMnO₄ were added into the above dispersion with ultrasound for 1 h. Afterwards the acid solution was heated in a microwave oven (Panasonic NN-GT337H, Shanghai, China) for 3 min and the process was repeated twice. The mixture was filtered and washed by deionized water until the solution was neutral. Finally, the MnO₂/CNT composite was obtained.

The 30 mg as-prepared MnO₂/CNT composite and 10 mg extra CNTs were further mixed and dispersed in ethanol. Then the mixture was drop-coated onto a piece of glass plate (2.5 × 7.5 cm²). After the ethanol was completely evaporated, the mixture of PCL and SMPU was dip-coated onto the conductive film. Subsequently, the composite was put into the oven at 70 °C for 12 h before being transferred to the vacuum for 12 h. Finally the self-healing conductive composite was peeled off and prepared. The prepared MnO₂/CNT/PCL/SMPU composite is denoted as MCP_xS_y, where x and y are the mass percent of PCL and SMPU, respectively.

The morphologies of CNT, MnO₂/CNT and MCPS were observed on a JEOL JSM-7001F scanning electron microscope (SEM, Tokyo, Japan). The structures of the samples were analyzed by X-ray Diffraction (XRD, D8 ADVANCE, Bruker, Germany). Differential Scanning Calorimetry (DSC, Perkin-Elmer Diamond, USA) and Raman spectroscopy (Raman, HORIBA Jobin Yvon LabRAMHR 800, Longjumeau, France) measurements were performed. The electrochemical behaviors of the composite were investigated by a CHI660D electrochemical workstation (Shanghai, Chen Hua). Cyclic voltammetry (CV) and chrono potentiometry (CP) techniques were utilized to study the electrochemical properties. The electrochemical performance of electrodes was conducted in a three-electrode system using a 1 M Na₂SO₄ aqueous solution as the electrolyte, with a conductive film as the working electrode, saturated calomel electrode (SCE) as the reference electrode and platinum wire as the counter electrode. The supercapacitors were fabricated via assembling two electrodes together in an area of 1 cm² with solid electrolyte, which was prepared by mixing 5 g H₂SO₄, 5 g PVA and 50 mL deionized water together at 85 °C until the solution was clear.

According to the charge/discharge curves and the CV curves, the specific capacitance (C, F cm⁻²) of a single electrode is calculated by the formula:

$$C = \frac{i \times t}{\Delta V \times S} \quad (1)$$

$$C = \frac{\int i x dV}{2v\Delta V \times S} \quad (2)$$

where *i* (mA cm⁻²) is the current density, *t* (s) is the discharge time, Δ*V* is the applied potential window, and *v* (mV s⁻¹) is the potential scan rate.

In order to quantitatively calculate the healing efficiency (η), Equation (3) is defined as follows:

$$\eta(\%) = \frac{C_{\text{healed}} - C_{\text{cracked}}}{C_{\text{pristine}} - C_{\text{cracked}}} \times 100 \quad (3)$$

where *C*_{pristine} is the capacitance of the pristine film and *C*_{healed} is the capacitance after self-healing. The capacitance of the cracked film (*C*_{cracked}) was obtained according to the capacitance equation. The self-healing efficiency (η) was calculated according to the capacitance data for samples at different states. Cracks in the width of several dozens of micrometers were manually generated by a scalpel or knife.

3. Results and Discussion

3.1. Fabrication and Morphologies of the Composite

The fabrication process of the healable conductive capacitors is schematically illustrated in Figure 1a, which contained three steps, namely co-reduction of the MnO₂ in the presence of the CNTs, re-dispersion of the decorated CNTs and integration of the healable polymer matrix. In the first step, the microwave treatment was an effective approach to reduce Mn⁷⁺ to Mn⁴⁺. After 3 min the resultant solution turned dark, which was indicative of the synthesis of the MnO₂ nano-particles. The decoration of the CNTs with the MnO₂ was expected to significantly increase the pseudocapacitance of the nano-carbon. However, it also decreased the dispersion of the CNTs. In order to ensure the decorated CNTs were well dispersed, a mixture of the decorated CNTs and the pristine CNTs at a ratio of 3:1 was necessary. It was found that the mixture suspension generated a homogeneous conductive film after the evaporation of the solvent, which was further embedded into the healable polymer matrix via the transfer process. Figure 1b shows the DSC measurements of the samples with different PCL contents. The changes in the peak areas became sharp and the melting temperature (*T*_m) of the PCL/SMPU shifted from 52.6 and 57.7 to 59.9 °C due to the increasing PCL contents. The shift of the *T*_m resulted from the strong interaction between the PCL and SMPU

components. The top-view and section-view scanning electron microscopy images in Figure 1c show the pure CNT (i), the as-prepared MnO_2/CNT (ii) and the healable conductive capacitive film (iii, iv). Image i shows that the CNTs were compactly entangled to form a mesh-like layer. For the nano composite MnO_2/CNT , a thin layer of MnO_2 nanoparticles was deposited on the CNT surfaces. Figure 1c(iii,iv) show the top and cross section views of the healable conductive capacitive film. It is obvious that the conductive layer was very well embedded into the polymer, of which the thickness was around 60 μm . Meanwhile, the increasing PCL contents led to the decrease in conduction. The conduction plots are shown in Figure 1d. The sheet resistances of the nano composite film were determined to be 8.44, 9.68 and 12.76 Ω/sq as the PCL contents were 20, 40 and 60 wt %, respectively. The composite exhibited superior flexibility, which is shown in Figure 2a,b. In order to measure the capacitance at different angles, the sample is bent and fixed. The coincident CV curves indicate that the composite could maintain the electrochemical performance at different bending angles. So, despite the deformation, the composite still had good capacitance. Figure 2b shows that sample MCP40S60 was connected into the DC circuit and then the LED could be lit up by applying 3V of voltage.

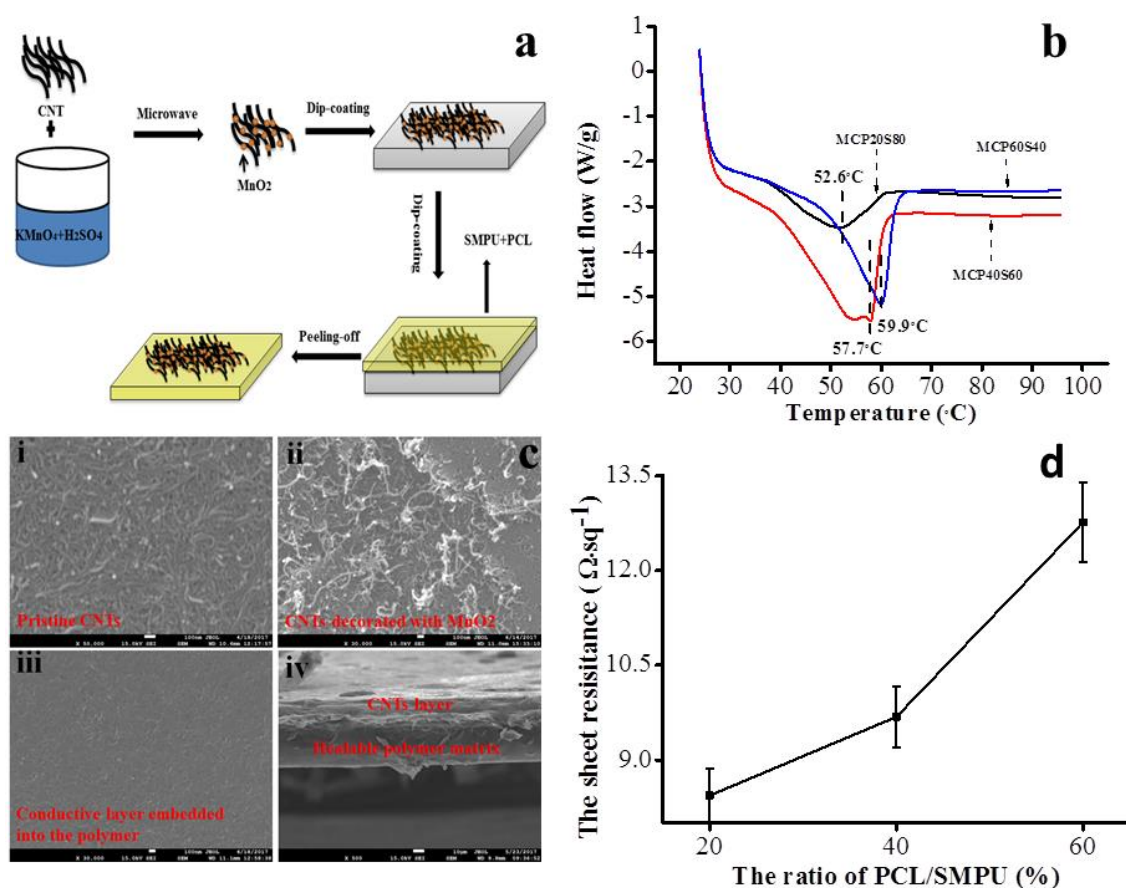


Figure 1. (a) Schematic diagram of the fabrication processes; (b) DSC curves of the samples with different PCL contents; (c) SEM images of the pure CNT (i), MnO_2/CNT (ii) as well as the surface (iii) and cross-section (iv) of the composite films; (d) sheet resistance of the composite with different PCL contents.

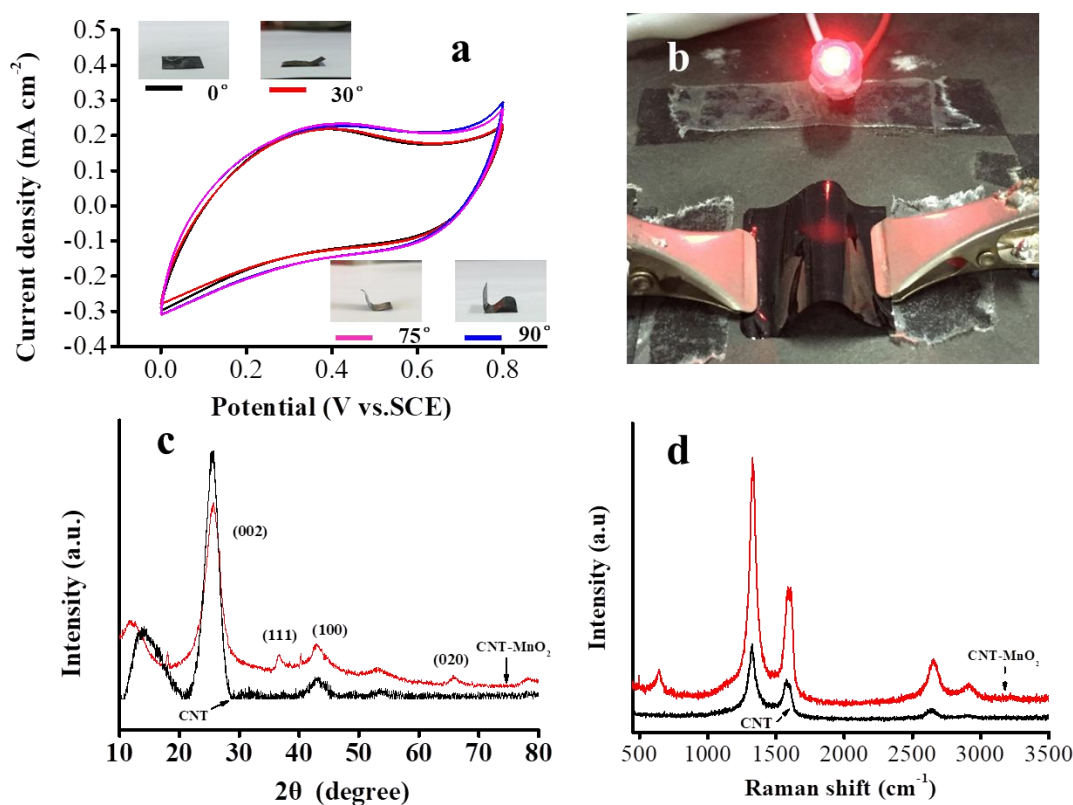


Figure 2. (a) CV curves of the composite at different bending angles at 5 mV s^{-1} ; (b) photographic demonstration of the sample MCP40S60 as the flexible composite; (c) XRD patterns of CNT and MnO_2/CNT ; (d) Raman spectra of CNT and MnO_2/CNT .

3.2. Capacitance Measurements of the Supercapacitors

Figure 2c shows the XRD patterns of the pure CNT and the as-prepared MnO_2/CNT composite. Two strong reflection peaks at 26° and 43.2° corresponding to the (002), (100) crystal plane of CNT, respectively, could be observed. From the XRD pattern of the as-prepared MnO_2/CNT composite, two weaker diffraction peaks could be indexed as the (111) and (020) diffraction bands, besides the stronger diffraction peaks corresponding to the (002) basal reflections. All of the reflection peaks were consistent with the reports on the tetragonal phase of $\alpha\text{-MnO}_2$ (JCPDS: 44-0141) [22]. Broad and weak peaks were assigned as the nanoscale characteristics of the synthesized $\alpha\text{-MnO}_2$, being indicative of the small crystal size and poor crystallinity of the composite. To further investigate the structural features of the MnO_2/CNT composite, Raman spectra of CNT and MnO_2/CNT composite were measured as shown in Figure 2d. There are three strong peaks at 1329 , 1558 , and 2652 cm^{-1} corresponding to the D, G, and 2D bands of CNT [23]. Compared to the Raman bands of pristine CNT, there is an obvious peak at 645 cm^{-1} corresponding to the symmetric stretching vibration (Mn-O) of the MnO_6 groups, which was consistent with the characteristics of tunnel species α -type MnO_2 materials [24].

Figure 3a displays the CV curves of the MCPS supercapacitors containing different contents of PCL recorded with the same sweep rate of 5 mV s^{-1} . The MCPS supercapacitors show good areal capacitances and similarity capacitance retentions. The galvanostatic charge-discharge curves of the MCP40S60 supercapacitors at various current densities ($0.2\text{--}1 \text{ mA cm}^{-2}$) are shown in Figure 3b. Based on the galvanostatic charge-discharge curves, the areal capacitances (Figure 3c) of the supercapacitors were calculated and plotted as a function of current densities. Clearly, the areal capacitance of 27.33 mF cm^{-2} was obtained by the MCP40S60 at a current density of 0.2 mA cm^{-2} . The CV and galvanostatic charge-discharge curves of MCP20S80 and MCP60S40 supercapacitors are shown in Figures S1 and S2. For the supercapacitors, another important parameter is the cycling

performance. The galvanostatic charge-discharge studies were performed at a current density of 0.6 mA cm^{-2} for 1500 cycles. It was calculated that the areal capacitance of MCP40S60 possessed good cycling stability and only 4.08% capacitance loss after 1500 cycles (Figure 3d).

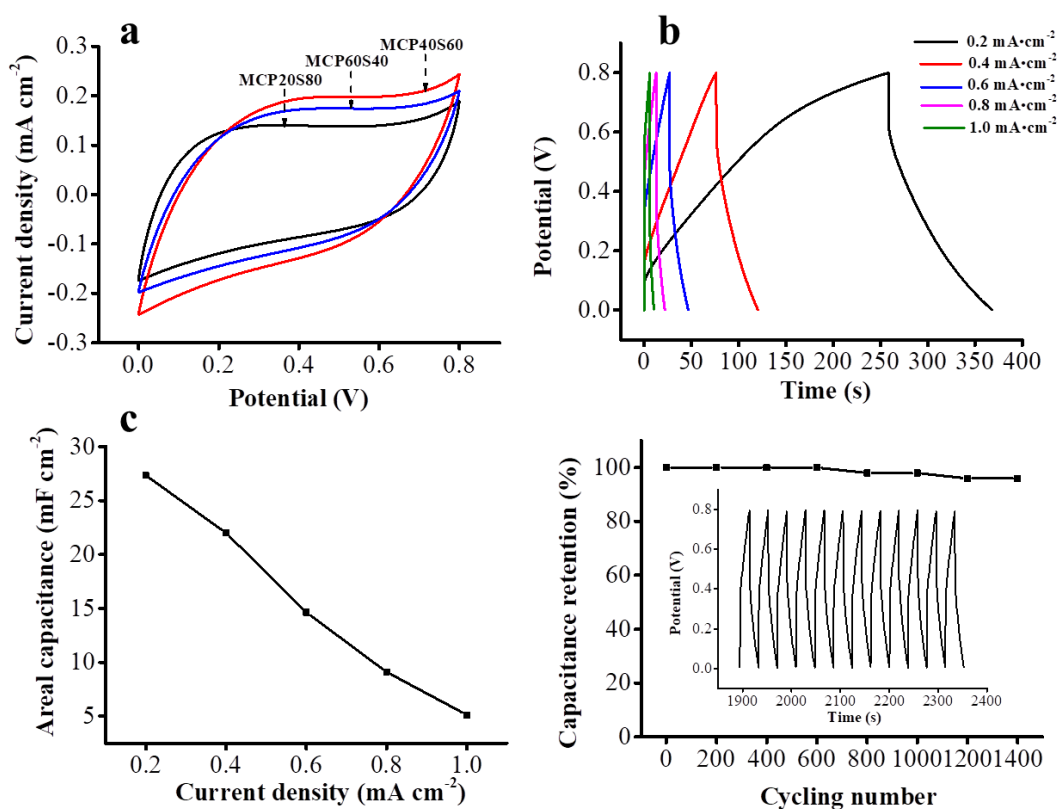


Figure 3. (a) CV curves of the supercapacitors with different PCL contents at 5 mV s^{-1} ; (b) galvanostatic charge/discharge curves of MCP40S60 supercapacitors collected at different current densities; (c) areal capacitances of MCP40S60 supercapacitors at different current densities; (d) cycle stability of MCP40S60 electrode film at 0.6 mA cm^{-2} .

3.3. Investigations on the Heal-Ability of the Electrodes

The PCL, as the healing reagent, not only played a critical role in the conduction of the composite, but also enhanced the self-healing of the composite. In order to disclose the thermal-triggered self-healing of the composite, CV measurements and galvanostatic charge-discharge measurements were performed. The CV measurements of MCP40S60, MCP20S80 and MCP60S40 at three different states were obtained at a sweep rate of 5 mV s^{-1} as shown in Figure 4a, Figures S3a and S4a. The galvanostatic charge-discharge measurements of MCP40S60, MCP20S80, and MCP60S40 at three different states were executed at a current density of 0.2 mA cm^{-2} as shown in Figure 4b, Figures S3b and S4b. When a scratch was made by a scalpel on the sample, most of the CNT/ MnO_2 were cut and broken along the crack, which led to a damaged conductive layer and decreased capacitance. However, the capacitance could be reversibly restored as the sample was heated because of the self-healing of the composite. The areal capacitances of the MCP40S60 electrode at a current density of 0.2 mA cm^{-2} were 5.8 mF cm^{-2} , $64.575 \text{ mF cm}^{-2}$, and 69 mF cm^{-2} , corresponding to the cracked, healed, and pristine state. The same results could be found from MCP20S80 and MCP60S40. This indicates that the composite with PCL possesses the excellent self-healing ability and the capacitance could be recovered even if it was scratched. According to the self-healing efficiency formula, the healing index of the MCPS electrode film is 85%, 93%, and 87%, respectively, as shown in Figure 4c. This implies that there exists an appropriate value of PCL content to obtain the optimal healing effect. The self-healing of the composite is resulted from the healing reagent PCL and the shape memory effect. It is well known

that PCL serves as a healing reagent in shape memory polymer systems, which experiences melting and recrystallization transitions during the healing process. The PCL can flow freely in the polymer as it heats up and fills in the defects of morphologies, and they are tightly bonded together as they cool. So as the PCL content increases, the more the melted PCL in the polymer matrix moves when it is heated, and the better the self-healing effect. To further verify the above discussion, a series of SEM images of the samples were taken. Figure 5 shows that the evolution of the surface morphologies under different contents of the PCL was monitored by SEM. A scratch with a width of dozens of micrometers was observed in the samples at the cracked states. However, heating at 60 °C for several minutes enabled the scratch to heal. The healing effect was improved with an increase in the PCL content. For instance, the samples with 40% and 60% of the PCL had better recovery under the thermal stimulations. What is more, heating not only made the PCL melt, but also triggered shape recovery enabling the cracked surface to be closer. The shape memory polymers are sensitive to temperature and high temperature endows them with good elasticity and shape recovery. So the shape memory effect contributed to the shrinking of the scratch and the melted PCL filled up the gap when the composite was healing. However, too much plastic PCL caused a lack of elastomeric force in the polymer matrix to drive the shape recovery as well as the crack closure. As a result, the sample containing 40 wt % of the PCL had optimized healable performance as the healable electrode.

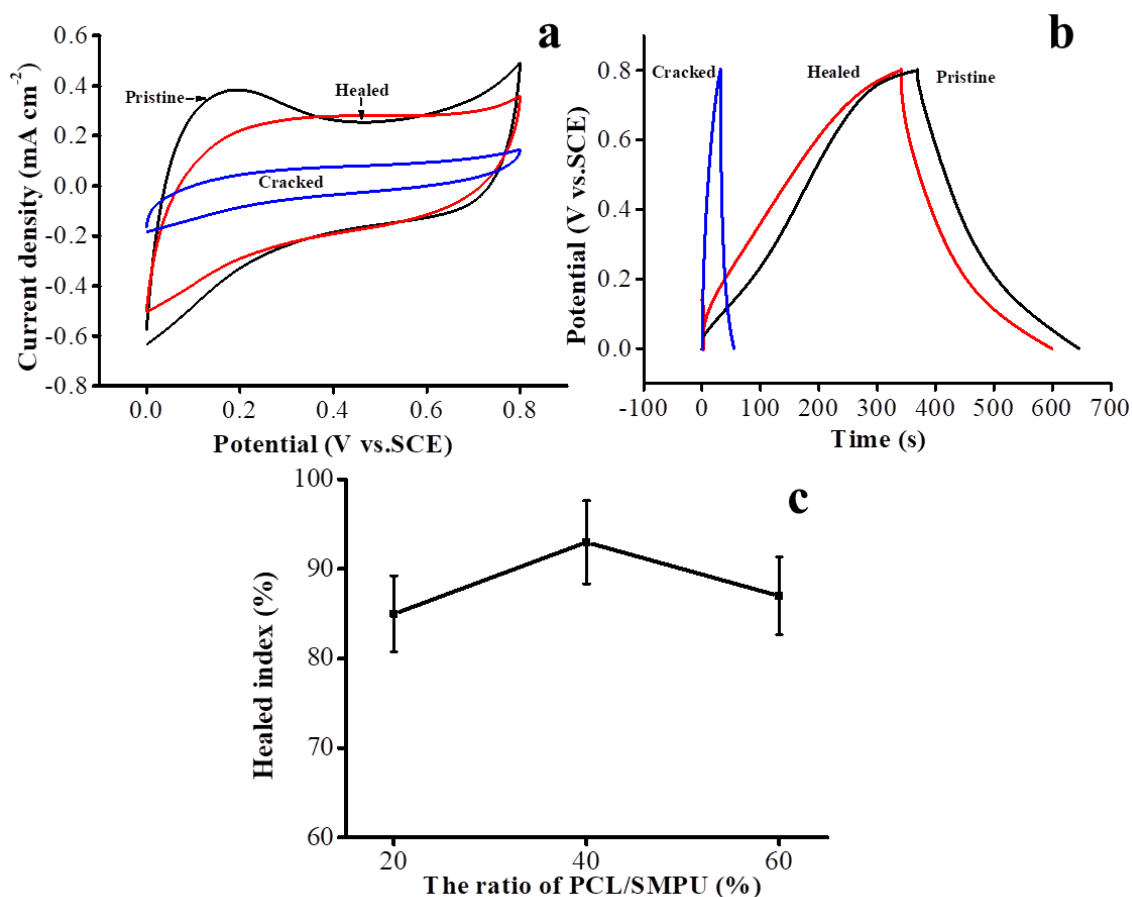


Figure 4. (a) CV curves of the MCP40S60 with different states collected at 5 mV s⁻¹; (b) galvanostatic charge/discharge curves of MCP40S60 electrode film with different states collected at 0.2 mA cm⁻²; (c) healed index of the composite with different PCL contents.

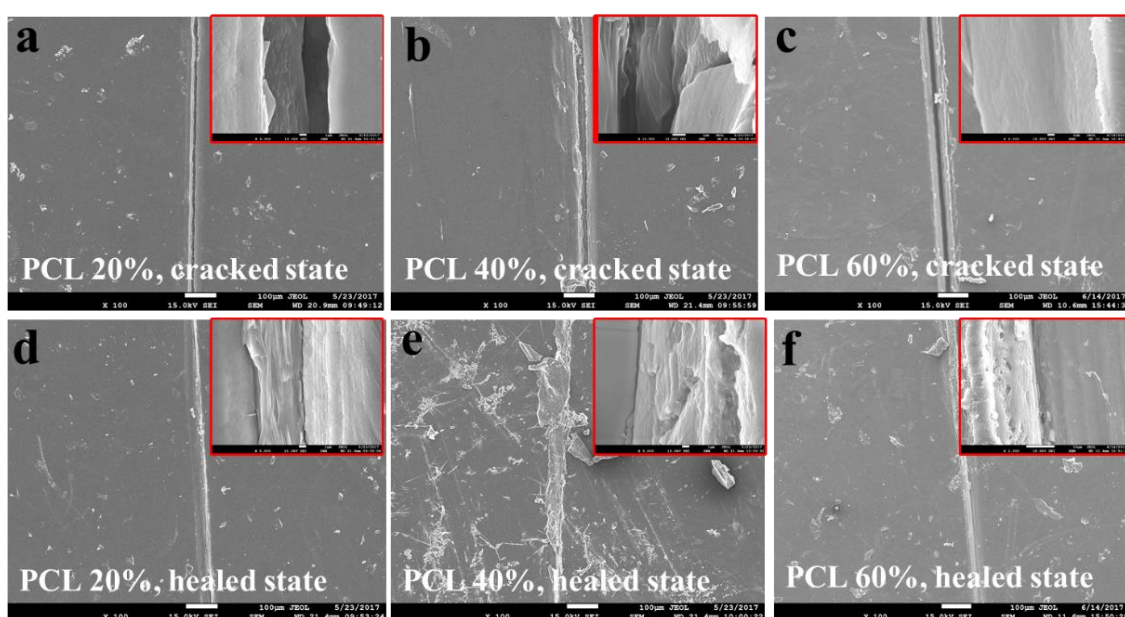


Figure 5. SEM images of the cracked areas before and after self-healing corresponding to 20% (a,d); 40% (b,e); 60% (c,f) PCL contents of the samples, respectively.

4. Conclusions

In summary, we successfully combined the MnO_2/CNT film with the mixture of PCL and SMPU substrate using transfer technology. We have demonstrated the fabrication of conductive MCPS films with good capacitance and thermal healability. The conductive MCP40S60 supercapacitors exhibit a good capacitance of 27.33 mF cm^{-2} at 0.2 mA cm^{-2} and cycle stability (1500 cycles with only 4.08% capacitance loss). The composite was capable of healing cracks under thermal stimulation once and excellent self-healing efficiency of up to 93% was obtained. Consequently, the superior performance of the MCPS electrode could contribute significantly to the design and fabrication of novel bio-mimetic supercapacitors.

Supplementary Materials: The following are available online at <http://www.mdpi.com/2076-3417/8/10/1732/s1>, Figure S1: (a) CV curves of the composite with 20% PCL contents collected at different scan rates; (b) galvanostatic charge/discharge curves of MCP20S80 electrode film; (c) areal capacitances of MCP20S80 electrode film at different current density. Figure S2: (a) CV curves of the composite with 60% PCL contents collected at different scan rates; (b) galvanostatic charge/discharge curves of MCP60S40 electrode film; (c) areal capacitances of MCP60S40 electrode film at different current density. Figure S3: (a) CV curves of the MCP20S80 at different states collected at 5 mV s^{-1} ; (b) galvanostatic charge/discharge curves of MCP20S80 electrode film at different states collected at 0.2 mA cm^{-2} . Figure S4: (a) CV curves of the MCP60S40 at different states collected at 5 mV s^{-1} ; (b) galvanostatic charge/discharge curves of MCP60S40 electrode film at different states collected at 0.2 mA cm^{-2} .

Author Contributions: Conceptualization, H.L. and H.Z.; Writing, H.Z.; Data curation, H.W.; Investigation, H.Z., X.Z. and Y.Y.; Formal analysis H.Z. and X.Z.; Resources, W.L. and G.Y.

Funding: This research received no external funding

Acknowledgments: The authors thank the Natural Science Foundation of China (No. 51873042), the China Postdoctoral Science Foundation (No. 2015M580709), and the Applied Science and Technology R&D and Provincial Open Laboratory Construction Foundation of Guangdong Province (Nos. 2017B090915004, 2017B030314105) for providing financial support.

Conflicts of Interest: The authors declare no conflict of interest.

References

1. Mather, P.T.; Luo, X.F.; Rousseau, I.A. Shape memory polymer research. *Annu. Rev. Mater. Res.* **2009**, *39*, 445–471. [[CrossRef](#)]
2. Rodriguez, E.D.; Luo, X.F.; Mather, P.T. Linear/network poly(epsilon-caprolactone) blends exhibiting shape memory assisted self-healing (smash). *ACS Appl. Mater. Interfaces* **2011**, *3*, 152–161. [[CrossRef](#)] [[PubMed](#)]
3. Luo, X.F.; Mather, P.T. Shape memory assisted self-healing coating. *ACS Macro Lett.* **2013**, *2*, 152–156. [[CrossRef](#)]
4. Mather, P.T.; Luo, X.F. Self-healing coatings utilizing a shape memory effect. In Proceedings of the 2013 ICSHM 4th International Conference on Self-Healing Materials, Ghent, Belgium, 16–20 June 2013.
5. Wei, H.Q.; Yao, Y.T.; Liu, Y.J.; Leng, J.S. A dual-functional polymeric system combining shape memory with self-healing properties. *Compos. Part B Eng.* **2015**, *83*, 7–13. [[CrossRef](#)]
6. Ge, J.; Cheng, G.H.; Chen, L.W. Transparent and flexible electrodes and supercapacitors using polyaniline/single-walled carbon nanotube composite thin films. *Nanoscale* **2011**, *3*, 3084–3088. [[CrossRef](#)] [[PubMed](#)]
7. Yuan, C.Z.; Yang, L.; Hou, L.R.; Shen, L.F.; Zhang, X.G.; Lou, X.W. Growth of ultrathin mesoporous Co₃O₄ nanosheet arrays on ni foam for high-performance electrochemical capacitors. *Energy Environ. Sci.* **2012**, *5*, 7883–7887. [[CrossRef](#)]
8. Lu, X.H.; Wang, G.M.; Zhai, T.; Yu, M.H.; Xie, S.L.; Ling, Y.C.; Liang, C.L.; Tong, Y.X.; Li, Y. Stabilized tin nanowire arrays for high-performance and flexible supercapacitors. *Nano Lett.* **2012**, *12*, 5376–5381. [[CrossRef](#)] [[PubMed](#)]
9. Huang, Y.; Zhong, M.; Huang, Y.; Zhu, M.S.; Pei, Z.X.; Wang, Z.F.; Xue, Q.; Xie, X.M.; Zhi, C.Y. A self-healable and highly stretchable supercapacitor based on a dual crosslinked polyelectrolyte. *Nat. Commun.* **2015**, *6*, 10310. [[CrossRef](#)] [[PubMed](#)]
10. Trivedi, T.J.; Bhattacharjya, D.; Yu, J.S.; Kumar, A. Functionalized agarose self-healing ionogels suitable for supercapacitors. *ChemsusChem* **2015**, *8*, 3294–3303. [[CrossRef](#)] [[PubMed](#)]
11. Wang, H.; Zhu, B.W.; Jiang, W.C.; Yang, Y.; Leow, W.R.; Wang, H.; Chen, X.D. A mechanically and electrically self-healing supercapacitor. *Adv. Mater.* **2014**, *26*, 3638–3643. [[CrossRef](#)] [[PubMed](#)]
12. Huang, Y.; Huang, Y.; Zhu, M.S.; Meng, W.J.; Pei, Z.X.; Liu, C.; Hu, H.; Zhi, C.Y. Magnetic-assisted, self-healable, yarn-based supercapacitor. *ACS Nano* **2015**, *9*, 6242–6251. [[CrossRef](#)] [[PubMed](#)]
13. Guo, Y.Z.; Zhou, X.; Tang, Q.Q.; Bao, H.; Wang, G.C.; Saha, P. A self-healable and easily recyclable supramolecular hydrogel electrolyte for flexible supercapacitors. *J. Mater. Chem. A* **2016**, *4*, 8769–8776. [[CrossRef](#)]
14. Zhou, X.D.; Luo, H.S.; Zhang, Y.H.; Wang, H.Q.; Lin, Y.L.; Zhao, G.R.; Yi, G.B.; Yuan, S.J.; Zhu, Z.Q. Tunable water sensitive polymeric composites with synergistic graphene and carbon nanotubes. *Mater. Lett.* **2017**, *199*, 160–163. [[CrossRef](#)]
15. Luo, H.S.; Zhou, X.D.; Ma, Y.Y.; Yi, G.B.; Cheng, X.L.; Zhu, Y.; Zu, X.H.; Zhang, N.J.; Huang, B.H.; Yu, L.F. Shape memory-based tunable resistivity of polymer composites. *Appl. Surf. Sci.* **2016**, *363*, 59–65. [[CrossRef](#)]
16. Luo, H.S.; Li, Z.W.; Yi, G.B.; Zu, X.H.; Wang, H.; Wang, Y.J.; Huang, H.L.; Hu, J.W.; Liang, Z.F.; Zhong, B.B. Electro-responsive silver nanowire-shape memory polymer composites. *Mater. Lett.* **2014**, *134*, 172–175. [[CrossRef](#)]
17. Yu, M.H.; Zhang, Y.F.; Zeng, Y.X.; Balogun, M.S.; Mai, K.C.; Zhang, Z.S.; Lu, X.H.; Tong, Y.X. Water surface assisted synthesis of large-scale carbon nanotube film for high-performance and stretchable supercapacitors. *Adv. Mater.* **2014**, *26*, 4724–4729. [[CrossRef](#)] [[PubMed](#)]
18. Zhang, Z.S.; Zhai, T.; Lu, X.H.; Yu, M.H.; Tong, Y.X.; Mai, K.C. Conductive membranes of eva filled with carbon black and carbon nanotubes for flexible energy-storage devices. *J. Mater. Chem. A* **2013**, *1*, 505–509. [[CrossRef](#)]
19. Zhi, J.; Reiser, O.; Huang, F.Q. Hierarchical MnO₂ spheres decorated by carbon-coated cobalt nanobeads: Low-cost and high-performance electrode materials for supercapacitors. *ACS Appl. Mater. Interfaces* **2016**, *8*, 8452–8459. [[CrossRef](#)] [[PubMed](#)]
20. Ma, Y.Y.; Yi, G.B.; Wang, J.C.; Wang, H.; Luo, H.S.; Zu, X.H. Shape-controllable and -tailorable multi-walled carbon nanotube/MnO₂/shape-memory polyurethane composite film for supercapacitor. *Synth. Met.* **2017**, *223*, 67–72. [[CrossRef](#)]

21. Zhu, Y.; Hu, J.L.; Yeung, K.W.; Choi, K.F.; Liu, Y.Q.; Liem, H.M. Effect of cationic group content on shape memory effect in segmented polyurethane cationomer. *J. Appl. Polym. Sci.* **2007**, *103*, 545–556. [[CrossRef](#)]
22. Wang, K.; Zhang, X.; Sun, X.Z.; Ma, Y.W. Conducting polymer hydrogel materials for high-performance flexible solid-state supercapacitors. *Sci. China Mater.* **2016**, *59*, 412–420. [[CrossRef](#)]
23. Banerjee, D.; Das, N.S.; Chattopadhyay, K.K. Enhancement of field emission and hydrophobic properties of silicon nanowires by chemical vapor deposited carbon nanoflakes coating. *Appl. Surf. Sci.* **2012**, *261*, 223–230. [[CrossRef](#)]
24. Gambou-Bosca, A.; Belanger, D. Chemical mapping and electrochemical performance of manganese dioxide/activated carbon based composite electrode for asymmetric electrochemical capacitor. *J. Electrochem. Soc.* **2015**, *162*, A5115–A5123. [[CrossRef](#)]



© 2018 by the authors. Licensee MDPI, Basel, Switzerland. This article is an open access article distributed under the terms and conditions of the Creative Commons Attribution (CC BY) license (<http://creativecommons.org/licenses/by/4.0/>).